
Article:
Muhammad, R., Iqbal, Y. and Reaney, I.M. (2016) BaTiO3–Bi(Mg2/3Nb1/3)O3 Ceramics for High-Temperature Capacitor Applications. Journal of the American Ceramic Society, 99 (6). pp. 2089-2095. ISSN 1551-2916

https://doi.org/10.1111/jace.14212

$BaTiO_3$–$Bi(Mg_{2/3}Nb_{1/3})O_3$ Ceramics for High Temperature Capacitor Applications

Raz Muhammad[a,c], Yaseen Iqbal[b] and Ian M Reaney[c]

[a]Department of Physics, Islamia College University of Peshawar, 25120 KP, Pakistan

[b]Materials Research Laboratory, Department of Physics, University of Peshawar, 25120 KP, Pakistan

[c]Department of Materials Science and Engineering, University of Sheffield, S1 3JD, UK

Email: razmohammad_phy@yahoo.com, dryaseeniqbal@yahoo.co.uk

Abstract

Solid solutions of $(1-x)BaTiO_3$–$xBi(Mg_{2/3}Nb_{1/3})O_3$ ($0 \leq x \leq 0.6$) were prepared via a standard mixed-oxide solid state sintering route and investigated for potential use in high-temperature capacitor applications. Samples with $0.4 \leq x \leq 0.6$ showed a temperature independent plateau in permittivity (ε_r). Optimum properties were obtained for $x = 0.5$ which exhibited a broad and stable relative $\varepsilon_r \sim 940 \pm 15\%$ from ~ 25°C to 550°C with a loss tangent < 0.025 from 74 to 455°C. The resistivity of samples increased with increasing $Bi(Mg_{2/3}Nb_{1/3})O_3$ concentration. The activation energies of the bulk were observed to increase from 1.18 to 2.25 eV with an increase in x from 0 to 0.6. These ceramics exhibited excellent temperature stable dielectric properties and are promising candidates for high temperature multilayer ceramic capacitors for automotive applications.

Keywords: Dielectric materials/properties; Electroceramics; Lead-free ceramics; Impedance spectroscopy

I. Introduction

Ceramic capacitors are the most extensively used components in modern electronic devices. Trillions of pieces of these ceramics are manufactured every year and hundreds of multilayer ceramic capacitors are used in typical electronic devices facilitating everyday life such as cell phones and computers.[1] The technological importance of a material can be recognized by its dielectric behavior and $BaTiO_3$, referred to as the cornerstone of the electroceramic market, is the base material for the majority of ceramic capacitors.[2] The Electrical Industries Association (EIA) designate the upper working temperature range of X7R, X8R and X9R capacitors as 125°C, 150°C and 200°C,

respectively, where X shows the lower operating temperature (X = -55°C) and R shows the variation in capacitance (i.e. ±15%).[3-5] The multifold increase in the use of electronic devices during the last few decades has significantly increased the demand for capacitors for applications in extreme environmental conditions. Such capacitors should be stable at temperatures approaching or exceeding 200°C, for example, for use in down-hole oil and natural gas explorations, aerospace and military equipment, and under-hood automotive electronics.[6, 7]

Pb-containing perovskite dielectrics are known to operate at temperatures higher than $BaTiO_3$-based but PbO is toxic and therefore Pb-free ceramics are preferred.[8, 9] Recent studies have therefore focused on Bi-based perovskite - $BaTiO_3$ solid solutions for the development of high temperature ceramic capacitors. Many such compounds show promising dielectric properties at > 200°C, including: $Bi(Mg_{1/2}Ti_{1/2})O_3$–$BaTiO_3$;[10] $BaTiO_3$–$BiScO_3$;[11] $BaTiO_3$–$Bi(Zn_{1/2}Ti_{1/2})O_3$–$BiScO_3$;[12] $Bi(Zn_{2/3}Nb_{1/3})O_3$–$(K_{0.5}Na_{0.5})NbO_3$;[13] $(1-x)Ba_{0.8}Ca_{0.2}TiO_3$–$xBi(Mg_{0.5}Ti_{0.5})O_3$;[14] $(1-x)Ba_{0.8}Ca_{0.2}TiO_3$–$xBi(Zn_{0.5}Ti_{0.5})O_3$;[15] $BaTiO_3$–$Bi(Mg_{0.5}Zr_{0.5})O_3$[16], $Bi_{0.5}Na_{0.5}TiO_3$–$NaNbO_3$[17] and $(Ba_{0.8}Ca_{0.2})TiO_3$–$Bi(Mg_{0.5}Ti_{0.5})O_3$–$NaNbO_3$.[18] All these solid solutions exhibit stable relative permittivities (ε_r) over a wide range of temperature. In some cases, temperature stable ε_r arises due to the overlap of two broad permittivity peaks while in others, structural and compositional heterogeneities have been reported to contribute to the flattening of ε_r,[14] as demonstrated by the core-shell grain structures identified in $BaTiO_3$–$BiScO_3$.[11]

Recently, $(1-x)BaTiO_3$–$xBi(Mg_{2/3}Nb_{1/3})O_3$ (x = 0.1) has been reported as a promising candidate material for high temperature capacitor applications due to its high ε_r (6800±15%) and low loss ($\tan\delta \leq 0.09$) at temperatures ranging from 25°C to 240°C (1 kHz).[19] Wang et al.[20] investigated the same $0.8BaTiO_3$–$0.2Bi(Mg_{2/3}Nb_{1/3})O_3$ system and reported relaxor-like behaviour with a temperature stable permittivity response from -50 to 300°C. This work was followed by Ma et al.[21] who processed $BaTiO_3$–$Bi(Mg_{2/3}Ta_{1/3})O_3$ solid solution for applications at lower temperatures but utilized more expensive Ta_2O_5 rather than Nb_2O_5. Here, we report the processing and dielectric properties of $(1-x)BaTiO_3$–$xBi(Mg_{2/3}Nb_{1/3})O_3$ in which $0.4 \leq x \leq 0.6$ exhibit a temperature independent plateau of ε_r up to high temperatures (>500 ^{o}C).

II. Experimental procedures

To prepare $(1-x)BaTiO_3$–$xBi(Mg_{2/3}Nb_{1/3})O_3$ ($0 \leq x \leq 0.6$) batch compositions, $BaCO_3$ (Sigma Aldrich, ≥99%), TiO_2 (Sigma Aldrich, ≥99%), Nb_2O_5 (Alfa Aesar, ≥99.5%), MgO (Sigma Aldrich, ≥99.9%) and Bi_2O_3 (Sigma Aldrich,

≥99.9%) were weighed in stoichiometric ratios. $BaCO_3$ and Bi_2O_3 were dried at 180°C while other oxides were heated at 800°C to remove moisture and hydroxides prior to batch preparation. All the batches were mixed-milled in polyethylene jars for 12 h, using isopropanol as lubricant and Y-toughened zirconia balls as grinding media. The resulting slurries were dried at 90°C overnight and then sieved. These powder samples were calcined in a muffle furnace at 900-1150°C for 6 h, at a heating/ cooling rate of 5°C/min. The calcined powder samples were re-milled using an agate mortar to dissociate agglomerates and pressed into ~ 3 mm high, 10 mm diameter cylindrical pellets using a uniaxial pellet press. The pellets were sintered at temperatures ranging from 1050 to 1350°C for 4h in air, at heating/cooling rate of 5°C/min. The density of the pellets was measured using a high precision electronic densitometer (Mettler Toledo, Switzerland). Phase analysis was carried out using a D5000 Siemens X-ray diffractometer (Germany), with CuKα = 1.5418 Å radiation. The lattice parameters were refined using least squares method. For electrical properties measurements, the opposite circular surfaces of sintered pellets were coated with gold paste and fired at 800°C for 2 h. The relative permittivity and dielectric loss at 1 kHz-1 MHz were measured in the temperature range ~ 25 to 550°C, using a HP 4284A precision LCR Meter (20 Hz -1 MHz). Impedance spectroscopy of these samples was carried out using a E4980A (Agilent) impedance analyzer at 20 Hz-2 MHz.

III. Results and discussion

The room temperature X-ray diffraction (XRD) patterns of $(1-x)BaTiO_3$-$xBi(Mg_{2/3}Nb_{1/3})O_3$ ($0 \leq x \leq 0.6$) samples sintered at their optimized temperatures are shown in Fig. 1. The XRD patterns at x = 0 (i.e. $BaTiO_3$) matched PDF# 01-074-1956 for the tetragonal (P4mm) $BaTiO_3$ phase. The splitting of the diffraction peak near $2\theta \sim 45°$ almost disappeared at $x \geq 0.05$ which suggested the formation of pseudo-cubic or cubic structures, consistent with the previous study.[19] The XRD patterns shifted towards lower 2θ which demonstrated an increase in lattice parameters and hence, an expansion of the unit cell (Fig. 2). No second phase peaks were observed within the detection limit of the in-house XRD, which confirmed the formation of a solid solution between $BaTiO_3$ and $Bi(Mg_{2/3}Nb_{1/3})O_3$ for $x \leq 0.6$. According to the principles of crystal chemistry and radius-matching rule, Bi^{+3} (1.36 Å)[22] ions are expected to occupy the A-site with r_{Ba+2} =1.61 Å [23] and Mg^{+2} (0.72 Å)[23] and Nb^{+5} (0.64 Å)[23] are expected to occupy the B-site with r_{Ti+4} = 0.605 Å [23] of the host lattice (equation 1).

$$Bi(Mg_{2/3}Nb_{1/3})O_3 \xrightarrow{\text{in } BaTiO_3 \text{ matrix}} Bi^{\bullet}_{Ba} + 3^{x}_{O} + 2/3Mg''_{Ti} + 1/3Nb^{\bullet}_{Ti} \rightarrow (1)$$

The addition of Bi^{3+} with $(Mg_{2/3}Nb_{1/3})^{3+}$ maintains charge neutrality without the formation of metal and/or oxygen vacancies.

Plots of ε_r and tanδ versus temperature measured at 1kHz-1MHz are shown in Fig. 3. The x = 0 compound exhibited a sharp Curie point (tetragonal-cubic phase transition i.e. T_c) near ~126°C with a large frequency dispersion at higher temperatures, typical behavior of un-doped $BaTiO_3$.[21] Broadening of the peak in ε_r was observed as x increased from 0.05 to 0.1 along with a shift in T_c to below room temperature. ε_r versus temperature flattened further with an increase in x (≥ 0.2) and showed relaxor-like behavior. Relaxor-like characteristics appear when a crystallographic site is shared by two cations which results in an increase in the random fields that inhibit the development of long range polar ordering.[20] In the present case, A-site and B-site were shared by two (Ba^{2+}, Bi^{3+}) and three cations (Ti^{4+}, Mg^{2+} and Nb^{5+}) respectively which may be the cause for the observed relaxor-like behavior. An anomalous behavior was observed for the x = 0.3 sample (Fig. 3) which showed a peak at ~ 475°C which may be associated with phase transition; however, the use of an alternate technique (like in-situ XRD, TEM or Raman) may be required to confirm the observed behavior.

Initially, the temperature (T_m) corresponding to the highest value of ε_r decreased from ~126°C (for x = 0) to ≤ 25°C (for 0.05-0.1 and then increased upon further increase in $Bi(Mg_{2/3}Nb_{1/3})O_3$ concentration (Table. 1). This kind of behavior has been previously reported for $BaTiO_3$-$Bi(Mg_{1/2}Ti_{1/2})O_3$ solid solutions and the initial depression of T_m has been attributed to the relatively less interaction of Bi^{3+}, Mg^{2+} and Ti^{4+} ions. After reaching at a certain level, the interaction of these ions enhanced and caused the observed high T_c character of BMT.[24] ε_r at T_m also decreased with an increase in x (Table 1).[19] Fig. 4 shows the percent (%) change in ε_r of $(1-x)BaTiO_3$-$xBi(Mg_{2/3}Nb_{1/3})O_3$ ($0.4 \leq x \leq 0.6$) solid solution as a function of temperature at 1 kHz. It is evident from Fig. 4 that the observed change in ε_r is within 15% over a wide temperature range for compositions with x > 0.3. The operating temperature ranges and dielectric loss of these compositions extracted from Fig. 3 are given in Table. 1 and compared with relevant data from previous studies.[10,12,14,19,21,25] Compositions with x = 0.5 were stable in the temperature range ~25°C to 550°C with a <15% change in ε_r ($\varepsilon_{r\ max}$ = 940) and tanδ < 0.025 (at 1 kHz) from 74 to 455°C whereas the operating temperature of compositions with x = 0.6 indicated <10% variation in ε_r in the temperature range 55°C to 543°C with $\varepsilon_{r\ max}$= 726.

Impedance spectroscopy (IS) is a powerful technique to investigate the electrical microstructure of ceramics.[26] The complex impedance plane plots (Z' versus Z'') showed two mutually overlapping electro-active regions for the $x \leq 0.1$ compositions. Fig. 5 shows the complex impedance plot of the x = 0 sample recorded at 450°C which was further followed by the spectroscopic plot M''/ε_o and Z'' as a function of frequency. The observed high frequency semi-circle or arc corresponds to the grain (i.e. bulk) while the low frequency arc corresponds to the grain boundary[27] which were further confirmed from the corresponding capacitances extracted from the plots (Fig. 5) using equation (2) and (3)

$$C = \frac{1}{2\pi \times f_{max(Z'')} R} \rightarrow (2)$$

$$C = \frac{1}{2M''_{max}/\varepsilon_o} \rightarrow (3)$$

The $x \geq 0.2$ samples showed a single arc which is believed to be associated with the grain because of the capacitance values ~ 10^{-11} F as shown for the typical composition with x = 0.6 at 750°C, Fig. 5.[27] The observed coincidence of the peaks in the plots of M'' and Z'' versus log(f) showed that the samples could be represented by a single parallel RC element in which both the total resistance and capacitance correspond to the bulk.[28] The observation of Debye-like single peaks at similar frequencies demonstrated the electrical homogeneity of the sample. The x = 0.5 sample exhibited the most promising properties; therefore, this sample was thoroughly investigated using IS (Fig. 6). Fig. 6a shows the Nyquist plots (Z' versus Z'') of the x = 0.5 sample which demonstrated a decrease in resistivity with an increase in temperature. A single semi-circular arc was observed at each temperature indicative of a single electro-active region. This was followed by the spectroscopic plots (M''/ε_o versus logf, Fig. 6b) with a single peak which shifted towards higher frequency with an increase in temperature. This observation indicated an increase in the mobility of charge carriers. To further investigate the electro-active region, a combined spectroscopic plot of Z'' and electric modulus M''/ε_o were examined which showed Debye-like single peaks at the employed frequencies (Fig. 6c). These observations demonstrated a homogenous electrical microstructure of the sample in the investigated temperature range. To find the nature of electro-active region, the capacitance values were also extracted (Fig. 6d). A small variation in the capacitance was observed in the range of 10^{-11} F, consistent with the capacitance of bulk ferroelectrics.[27] The decreasing trend in resistivity (Fig. 6d) with increasing temperature gave a negative temperature

coefficient of resistivity (NTCR), a typical semi-conducting behavior. The temperature dependence of conductivity indicated that the ionic conduction may be responsible for the observed increase in conductivity and oxygen vacancy was the most mobile ionic defect. Arrhenius plots of σ_g and σ_{gb} were extracted from M''/ε_o and Z'' spectroscopic plots which were also used to determine the activation energy associated with conduction, given by equation (4)

$$\sigma = \sigma_o e^{\frac{-E_a}{K_B T}} \rightarrow (4)$$

Where σ_o is the pre-exponential factor, K_B is the Boltzmann's constant, T is temperature, and E_a is the activation energy. E_a was calculated from the slope of log(σ) versus 1000/T. The conductivity of the $x \geq 0.2$ samples was ~ 10^{-7} S/cm at 600°C, suggesting the highly insulating behavior with activation energies ranging from 1.58 to 2.25 eV (Table 2), calculated from the slope in Fig. 7. The composition with x = 0.4 showed an anomalous but the discrepancy could not be understand and might need further investigations (Table 2). The motion of oxygen vacancies give rise to activation energy and are considered as the most mobile charge carriers in perovskite ferroelectrics.[29] These vacancies create conducting electrons which can be easily activated thermally; however, the present activation energies for conduction for samples $x \leq 0.2$ suggested the possibility of electrical conduction due to the mobility of oxygen ions (O^{2-}) or oxygen ion vacancies V_O'' at higher temperatures and hence ionic conduction may be responsible for the degradation of resistivity at higher temperatures.[29, 30] However, the large activation energies of samples $x \geq 0.03$ suggest an intrinsic conduction mechanism i.e. carrier excitation across an intrinsic band gap.[31, 32] Nonetheless, the compounds with $0.4 \leq x \leq 0.6$ could be ideal candidate materials for high voltage and high temperature power applications[33] due to their low dielectric loss and temperature stable relative permittivity over a wide temperature range.

IV. Conclusions

(1-x)$BaTiO_3$–x$Bi(Mg_{2/3}Nb_{1/3})O_3$ (x = 0-0.6) solid solutions were processed through a conventional mixed-oxide solid state sintering route. Compositions with $0.4 \leq x \leq 0.6$ exhibited a temperature independent ε_r over a broad temperature range. The resistivity of these samples increased with increasing $Bi(Mg_{2/3}Nb_{1/3})O_3$ concentration, commensurate with an increase in bulk activation energies from 1.18 to 2.25 eV. However, the conductivity increased with an increase in temperature indicating semiconducting behavior at higher temperatures (≥ 500°C). The low dielectric

loss and temperature stable ε_r make (1-x)$BaTiO_3$–x$Bi(Mg_{2/3}Nb_{1/3})O_3$ solid solutions with $0.4 \leq x \leq 0.6$ potential candidates for high temperature capacitor applications.

Acknowledgments

The authors acknowledge the Higher Education Commission (HEC) of Pakistan for research fellowship under the International Research Support Initiative Program (IRSIP) to Dr. R. Muhammad at the Department of Materials Science and Engineering, University of Sheffield, UK. The financial support extended by the Directorate of S&T, KP via ADP No. 130314 is equally acknowledged for the enhancement of research facilities in Materials Research Laboratory, University of Peshawar.

References

[1]M.-J. Pan and C. A. Randall, "A brief introduction to ceramic capacitors," Electrical Insulation Magazine, IEEE, **26** [3] 44-50 (2010).

[2]C. L. Freeman, J. A. Dawson, J. H. Harding, L. B. Ben and D. C. Sinclair, "The Influence of A-Site Rare Earth Ion Size in Controlling the Curie Temperature of $Ba_{1-x}RE_xTi_{1-x/4}O_3$," Adv. Func. Mater., **23** [4] 491-495 (2013).

[3]S. Gao, S. Wu, Y. Zhang, H. Yang and X. Wang, "Study on the microstructure and dielectric properties of X9R ceramics based on $BaTiO_3$," Mater. Sci. Eng. B, **176** [1] 68-71 (2011).

[4]S.-F. Wang, J.-H. Li, Y.-F. Hsu, Y.-C. Wu, Y.-C. Lai and M.-H. Chen, "Dielectric properties and microstructures of non-reducible high-temperature stable X9R ceramics," J. Eur. Ceram. Soc., **33** [10] 1793-1799 (2013).

[5]L.-x. Li, Y.-m. Han, P. Zhang, C. Ming and X. Wei, "Synthesis and characterization of $BaTiO_3$-based X9R ceramics," J. Mater. Sci., **44** [20] 5563-5568 (2009).

[6]Pat Hollenbeck, "Capacitor Technology Options for High Temperature and Harsh Environment Applications," CARTS International, (2014).

[7]A. Zeb and S. Milne, "High temperature dielectric ceramics: a review of temperature-stable high-permittivity perovskites," J. Mater. Sci.: Mater. Electron., **26** [12] 9243-9255 (2015).

[8]V. V. Shvartsman and D. C. Lupascu, "Lead-Free Relaxor Ferroelectrics," J. Am. Ceram. Soc., **95** [1] 1-26 (2012).

[9]Y. Li, K.-s. Moon and C. Wong, "Electronics without lead," Science, **308** [5727] 1419-1420 (2005).

[10]Q. Zhang, Z. Li, F. Li and Z. Xu, "Structural and Dielectric Properties of $Bi(Mg_{1/2}Ti_{1/2})O_3$–$BaTiO_3$ Lead-Free Ceramics," J. Am. Ceram. Soc., **94** [12] 4335-4339 (2011).

[11]H. Ogihara, C. A. Randall and S. Trolier-McKinstry, "High-Energy Density Capacitors Utilizing $0.7BaTiO_3$–$0.3BiScO_3$ Ceramics," J. Am. Ceram. Soc., **92** [8] 1719-1724 (2009).

[12]N. Raengthon, T. Sebastian, D. Cumming, I. M. Reaney and D. P. Cann, "$BaTiO_3$–$Bi(Zn_{1/2}Ti_{1/2})O_3$–$BiScO_3$ Ceramics for High-Temperature Capacitor Applications," Journal of the American Ceramic Society, **95** [11] 3554-3561 (2012).

[13]H. Cheng, H. Du, W. Zhou, D. Zhu, F. Luo and B. Xu, "$Bi(Zn_{2/3}Nb_{1/3})O_3$–$(K_{0.5}Na_{0.5})NbO_3$ High-Temperature Lead-FreeFerroelectric Ceramics with Low Capacitance Variation in a Broad Temperature Usage Range," J. Am. Ceram. Soc., **96** [3] 833-837 (2013).

[14]A. Zeb and S. J. Milne, "Stability of High-Temperature Dielectric Properties for $(1-x)Ba_{0.8}Ca_{0.2}TiO_3$–$xBi(Mg_{0.5}Ti_{0.5})O_3$ Ceramics," J. Am. Ceram. Soc., **96** [9] 2887-2892 (2013).

[15]A. Zeb and S. J. Milne, "Low variation in relative permittivity over the temperature range 25–450° C for ceramics in the system $(1-x)[Ba_{0.8}Ca_{0.2}TiO_3]$–$x[Bi(Zn_{0.5}Ti_{0.5})O_3]$," J. Eur. Ceram. Soc., **34** [7] 1727-1732 (2014).

[16]A. Zeb and S. J. Milne, "Temperature-stable dielectric properties from− 20° C to 430° C in the system $BaTiO_3$–$Bi(Mg_{0.5}Zr_{0.5})O_3$," J. Eur. Ceram. Soc., **34** [13] 3159-3166 (2014).

[17]Q. Xu, Z. Song, W. Tang, H. Hao, L. Zhang, M. Appiah, M. Cao, Z. Yao, Z. He and H. Liu, "Ultra-Wide Temperature Stable Dielectrics Based on $Bi_{0.5}Na_{0.5}TiO_3$–$NaNbO_3$ System," J. Am. Ceram. Soc., **98** [10] 3119-3126 (2015).

[18]A. Zeb, Y. Bai, T. Button and S. J. Milne, "Temperature-Stable Relative Permittivity from −70° C to 500° C in $(Ba_{0.8}Ca_{0.2})TiO_3$–$Bi(Mg_{0.5}Ti_{0.5})O_3$–$NaNbO_3$ Ceramics," J. Am. Ceram. Soc., **97** [8] 2479-2483 (2014).

[19]X. Chen, J. Chen, D. Ma, L. Fang and H. Zhou, "Thermally Stable $BaTiO_3$-$Bi(Mg_{2/3}Nb_{1/3})O_3$ Solid Solution with High Relative Permittivity in a Broad Temperature Usage Range," J. Am. Ceram. Soc., **98** [3] 804-810 (2015).

[20]T. Wang, L. Jin, C. Li, Q. Hu and X. Wei, "Relaxor Ferroelectric $BaTiO_3$–$Bi(Mg_{2/3}Nb_{1/3})O_3$ Ceramics for Energy Storage Application," J. Am. Ceram. Soc., **98** [2] 559-566 (2015).

[21]D. Ma, X. Chen, G. Huang, J. Chen, H. Zhou and L. Fang, "Temperature stability, structural evolution and dielectric properties of $BaTiO_3$–$Bi(Mg_{2/3}Ta_{1/3})O_3$ perovskite ceramics," Ceram. Int., **41** [5] 7157-7161 (2015).

[22]C. W. Tai, S. H. Choy and H. L. Chan, "Ferroelectric Domain Morphology Evolution and Octahedral Tilting in Lead-Free $(Bi_{1/2}Na_{1/2})TiO_3$–$(Bi_{1/2}K_{1/2})TiO_3$–$(Bi_{1/2}Li_{1/2})TiO_3$–$BaTiO_3$ Ceramics at Different Temperatures," J. Am. Ceram. Soc., **91** [10] 3335-3341 (2008).

[23]R. D. Shannon, "Revised effective ionic radii and systematic studies of interatomic distances in halides and chalcogenides," Acta Crystallogr. Sec. A, **32** [5] 751-767 (1976).

[24]Bo Xiong, Hua Hao, Shujun Zhang, Hanxing Liu and Minghe Cao, "Structure, Dielectric Properties and Temperature Stability of $BaTiO_3$–$Bi(Mg_{1/2}Ti_{1/2})O_3$ Perovskite Solid Solutions," J. Am. Ceram. Soc., **94** [10] 3412–3417 (2011).

[25]S. Wada, K. Yamato, P. Pulpan, N. Kumada, B.-Y. Lee, T. Iijima, C. Moriyoshi and Y. Kuroiwa, "Piezoelectric properties of high Curie temperature barium titanate–bismuth perovskite-type oxide system ceramics," J. Appl. Phys., **108** [9] 094114 (2010).

[26]A. R. West, D. C. Sinclair and N. Hirose, "Characterization of electrical materials, especially ferroelectrics, by impedance spectroscopy," J. Electroceram., **1** [1] 65-71 (1997).

[27]J. T. Irvine, D. C. Sinclair and A. R. West, "Electroceramics: characterization by impedance spectroscopy," Adv. Mater., **2** [3] 132-138 (1990).

[28]N. Maso, H. Beltran, E. Cordoncillo, A. A. Flores, P. Escribano, D. Sinclair and A. West, "Synthesis and electrical properties of Nb-doped $BaTiO_3$," J. Mater. Chem., **16** [30] 3114-3119 (2006).

[29]S. Sen, R. Choudhary and P. Pramanik, "Structural and electrical properties of Ca^{2+}-modified PZT electroceramics," Physica B, **387** [1] 56-62 (2007).

[30]M. Ramesh and K. Ramesh, "Dielectric and impedance spectroscopic studies of 0.8 $BaTiO_3$–$0.2Bi_{0.5}K_{0.5}TiO_3$ lead-free ceramics," Int. J. Mod. Phys. B, **29** [18] 1550119 (2015).

[31]N. Raengthon and D. P. Cann, "Dielectric relaxation in $BaTiO_3$–Bi $(Zn_{1/2}Ti_{1/2})O_3$ ceramics," J. Am. Ceram. Soc., **95** [5] 1604-1612 (2012).

[32]R. Rawal, A. Feteira, N. C. Hyatt, D. C. Sinclair, K. Sarma and N. M. Alford, "Microwave Dielectric Properties of Hexagonal 12R-$Ba_3LaNb_3O_{12}$ Ceramics," J. Am. Ceram. Soc., **89** [1] 332-335 (2006).

[33]D. H. Choi, A. Baker, M. Lanagan, S. Trolier-McKinstry and C. Randall, "Structural and Dielectric Properties in $(1-x)BaTiO_3–xBi(Mg_{1/2}Ti_{1/2})O_3$ Ceramics ($0.1\leq x\leq 0.5$) and Potential for High-Voltage Multilayer Capacitors," Journal of the American Ceramic Society, **96** [7] 2197-2202 (2013).

Table 1. Dielectric properties of (1-x)$BaTiO_3$–x$Bi(Mg_{2/3}Nb_{1/3})O_3$ (x = 0.3-0.6)

Sample	T_m (°C) (1 kHz)	$\varepsilon_{r\,(max)}$ (1 kHz)	T-range (°C) $\varepsilon_r \pm 10\%$ (1kHz)	T-range (°C) $\varepsilon_r \pm 15\%$ (1kHz)	T-range (°C) tanδ < 0.025 (1kHz)
BT-BMNb (x = 0.3) present work	30	1010	151-350 $\varepsilon_r = 857\pm10$	77-395 $\varepsilon_r = 857\pm15$	45-437
BT-BMNb (x = 0.4)	87	1007	~ 25-472 $\varepsilon_r = 933\pm10$	~ 25-550 $\varepsilon_r = 933\pm15$	57-380
BT-BMNb (x = 0.5) present work	96	974	40-487 $\varepsilon_r = 940\pm10$	34-550 $\varepsilon_r = 940\pm15$	74-455
BT-BMNb (x = 0.6) present work	106	737	55-543 726	44-550 $\varepsilon_r = 726\pm15$	87-350
0.5BCT-0.5BMT[13]	120	875	45-550 $\varepsilon_r = 800\pm10$	--	100-430
0.5BT-0.25BZT-0.25BS (Ba-deficient)[11]	100	1000-1100	100-500 $\varepsilon_r = 1100\pm10$	--	100-450
0.6BT-0.4BMT[9]	200	2000	200-400 $\varepsilon_r = 2000\pm10$	--	200-400
0.85BT–0.15BMT+2wt% Nb_2O_5[23]	14 & 130	900	-55-155 $\varepsilon_r = 900\pm10$	--	0-200
0.9BT-0.1BMTa[19]	~ 25 &130	1278	--	30-150 $\varepsilon_r = 1278$	30-198 (tanδ < 0.02)
0.9BT-0.1BMNb[17]	--	6800	--	20-240±15 $\varepsilon_r = 6800\pm15$	30-198 (tanδ < 0.09)

*BCT-BMT ($Ba_{0.8}Ca_{0.2}TiO_3$-$BiMg_{0.5}Ti_{0.5}O_3$), BT-BZT-BS ($BaTiO_3$-$BizZn_{0.5}Ti_{0.5}O_3$-$BiScO_3$), BT-BMT ($BaTiO_3$-$BiMg_{0.5}Ti_{0.5}O_3$), BT-BMTa ($BaTiO_3$–x$BiMg_{2/3}Ta_{1/3}O_3$), BT-BMNb ($BaTiO_3$–x$BiMg_{2/3}Nb_{1/3}O_3$)

Table 2. Activation energies of bulk (E_b) and grain boundary (E_{gb}), resistivities (ρ_b) and conductivities (σ_b) of bulk at 600°C

x	0	0.05	0.1	0.2	0.3	0.4	0.5	0.6
E_g/E_{gb} (eV)	1.18/1.45	1.16/1.24	1.30/1.47	1.58	1.87	1.93	2.24	2.25
ρ_b (Ω-cm)	*4.8×10^3	*9.4×10^3	8.3×10^3	1.4×10^6	5.4×10^6	7.53×10^5	6×10^6	6.2×10^6
σ_b (S/cm^{-1})	*2.1×10^{-4}	*1.1×10^{-4}	1.2×10^{-4}	7.2×10^{-7}	1.8×10^{-7}	1.32×10^{-6}	1.7×10^{-7}	1.6×10^{-7}

*(500°C)

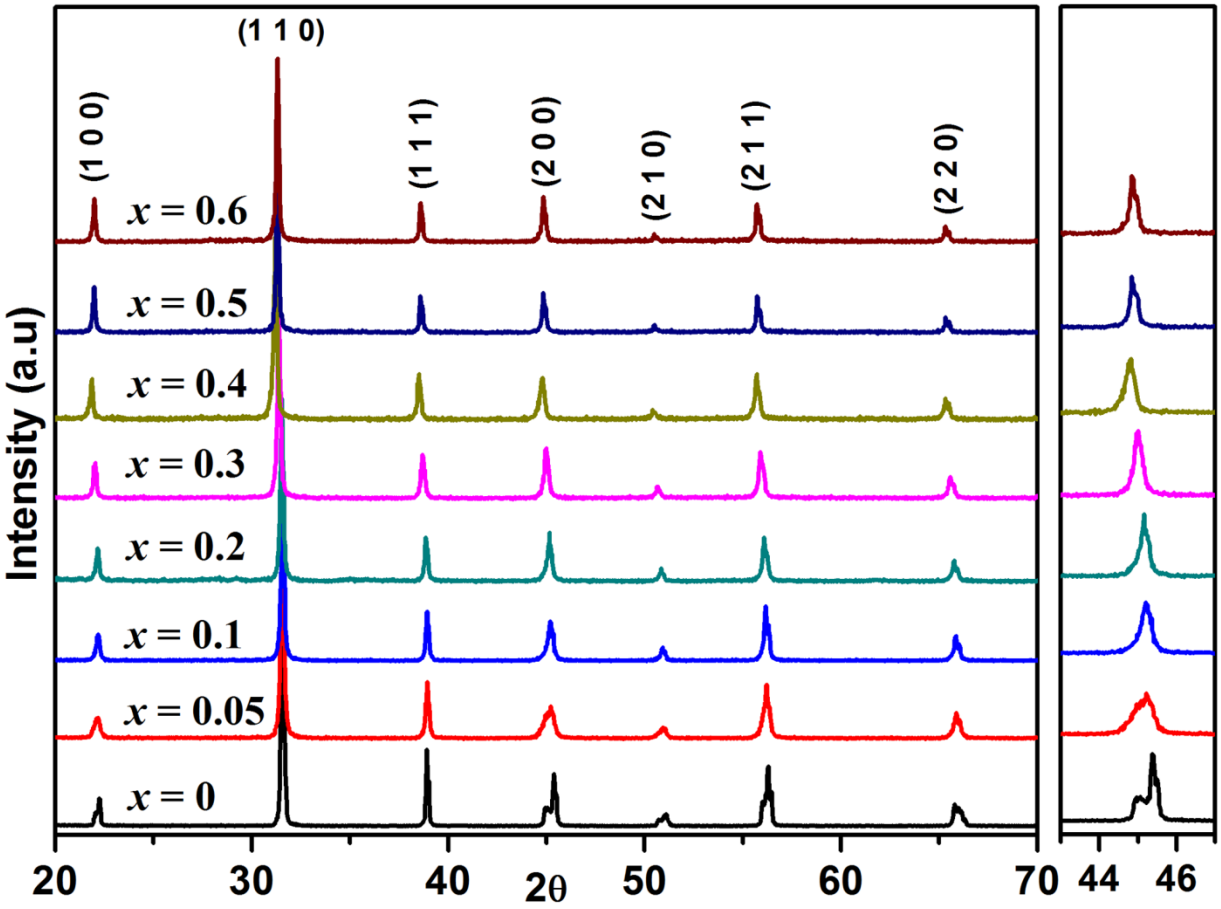

Fig. 1. Room temperature XRD patterns of (1-x)$BaTiO_3$–x$Bi(Mg_{2/3}Nb_{1/3})O_3$ (x = 0-0.6) sintered at their optimum temperatures

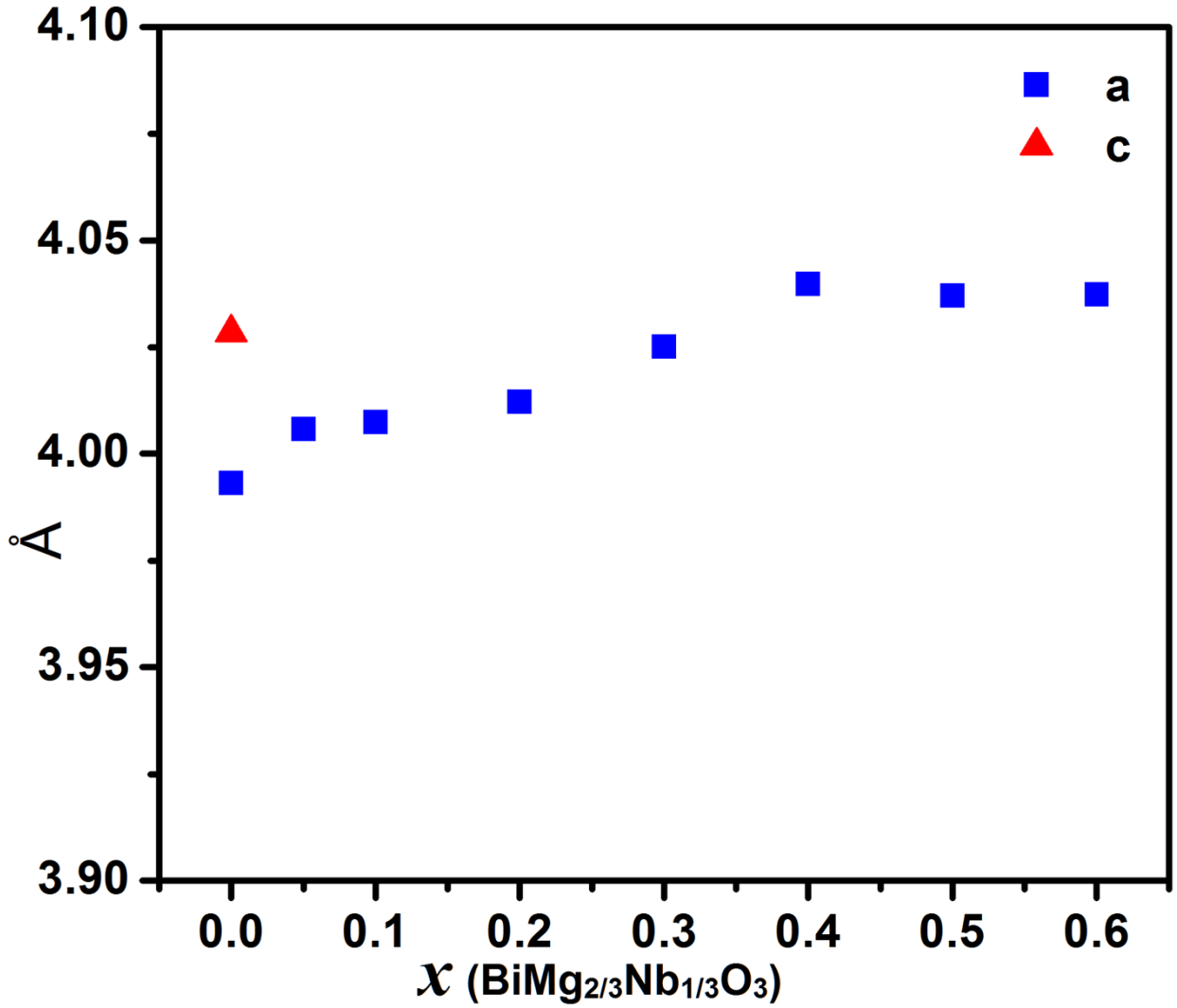

Fig. 2. Lattice parameters of (1-x)$BaTiO_3$–x$Bi(Mg_{2/3}Nb_{1/3})O_3$ (x = 0-0.6)

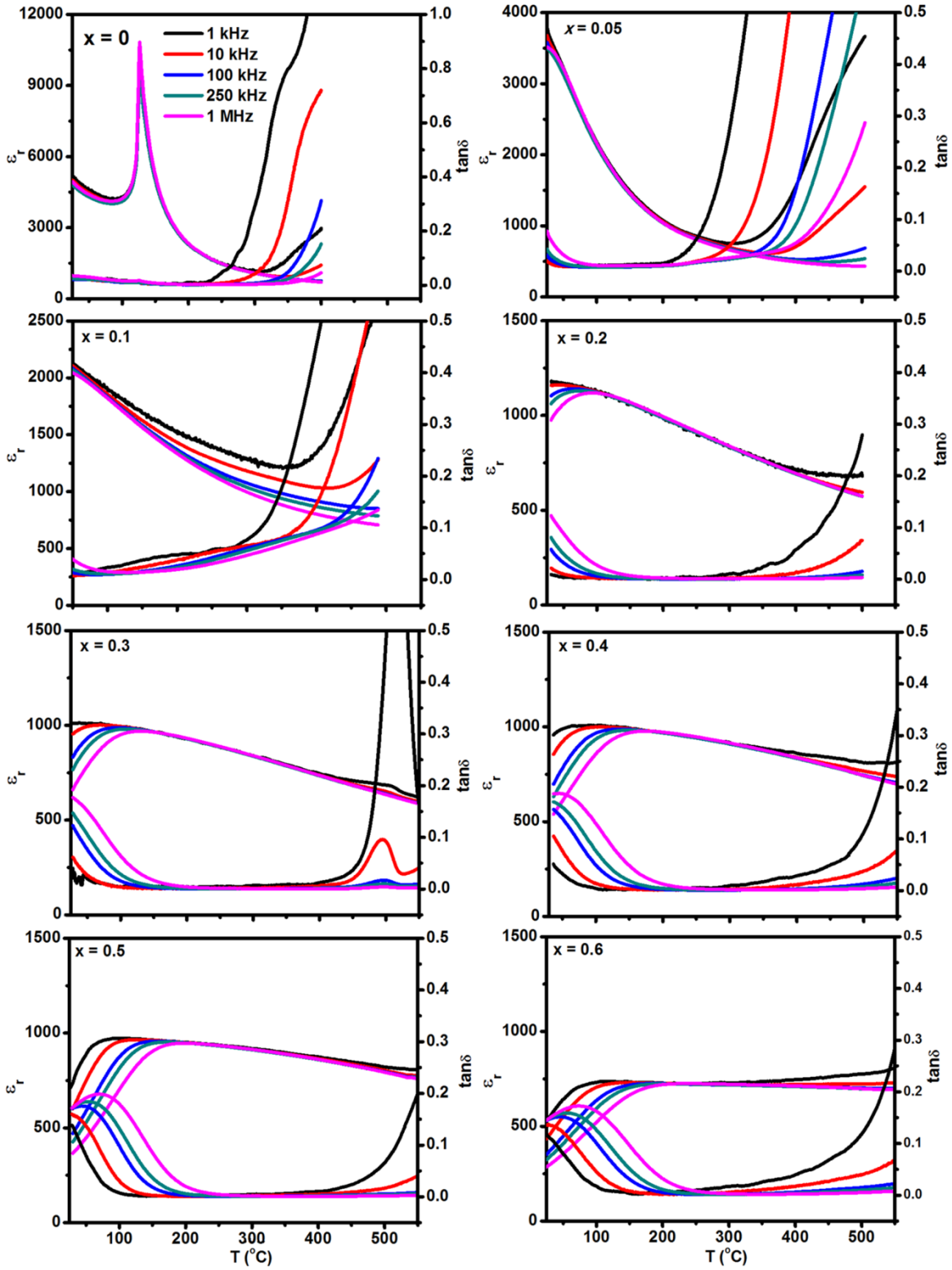

Fig. 3. ε_r and tanδ versus temperature plots for (1-x)$BaTiO_3$–x$Bi(Mg_{2/3}Nb_{1/3})O_3$ at 1 kHz–1 MHz

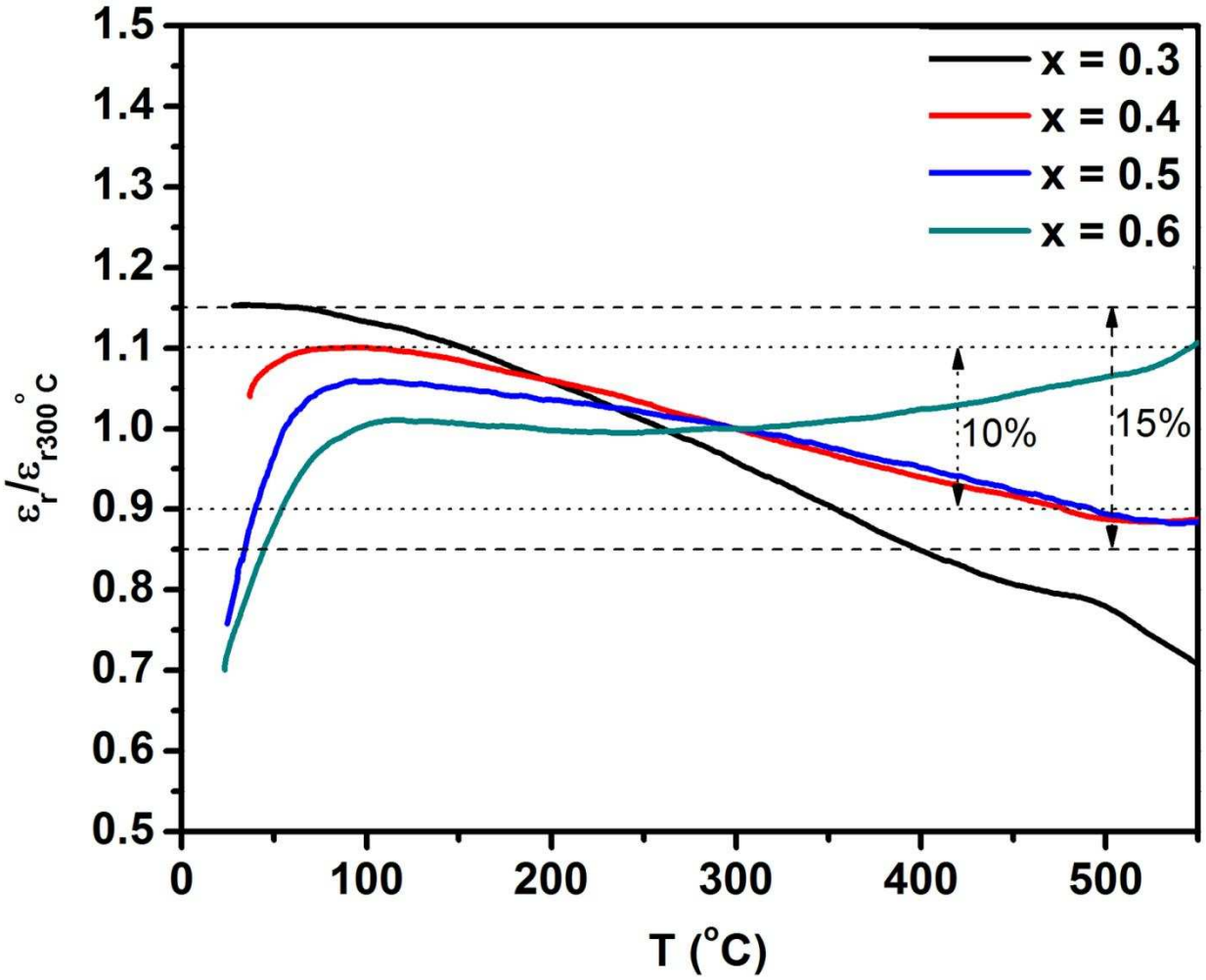

Fig. 4. Change in relative permittivity as a function of temperature for (1-x)$BaTiO_3$–x$Bi(Mg_{2/3}Nb_{1/3})O_3$ (x = 0.3-0.6)

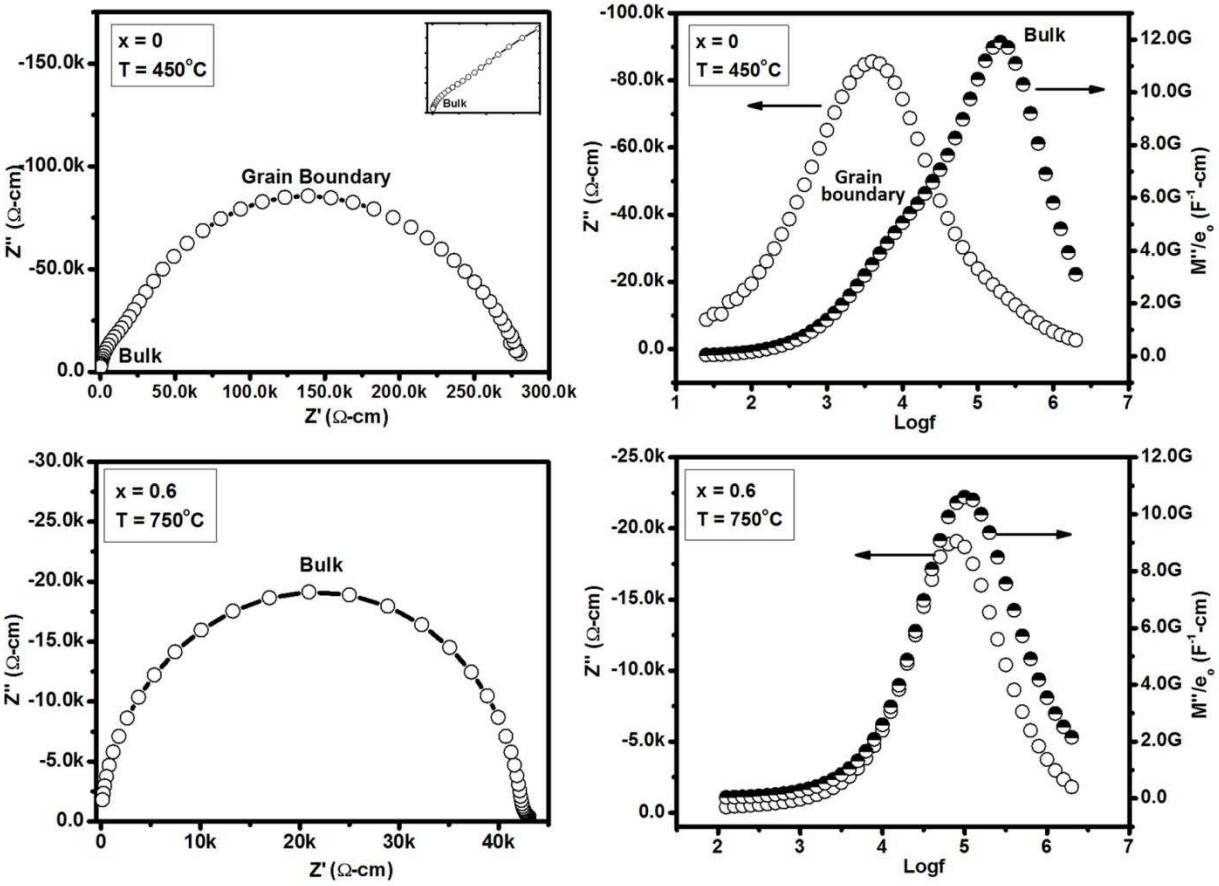

Fig. 5. Impedance spectroscopic plots of samples x = 0 and x = 0.6

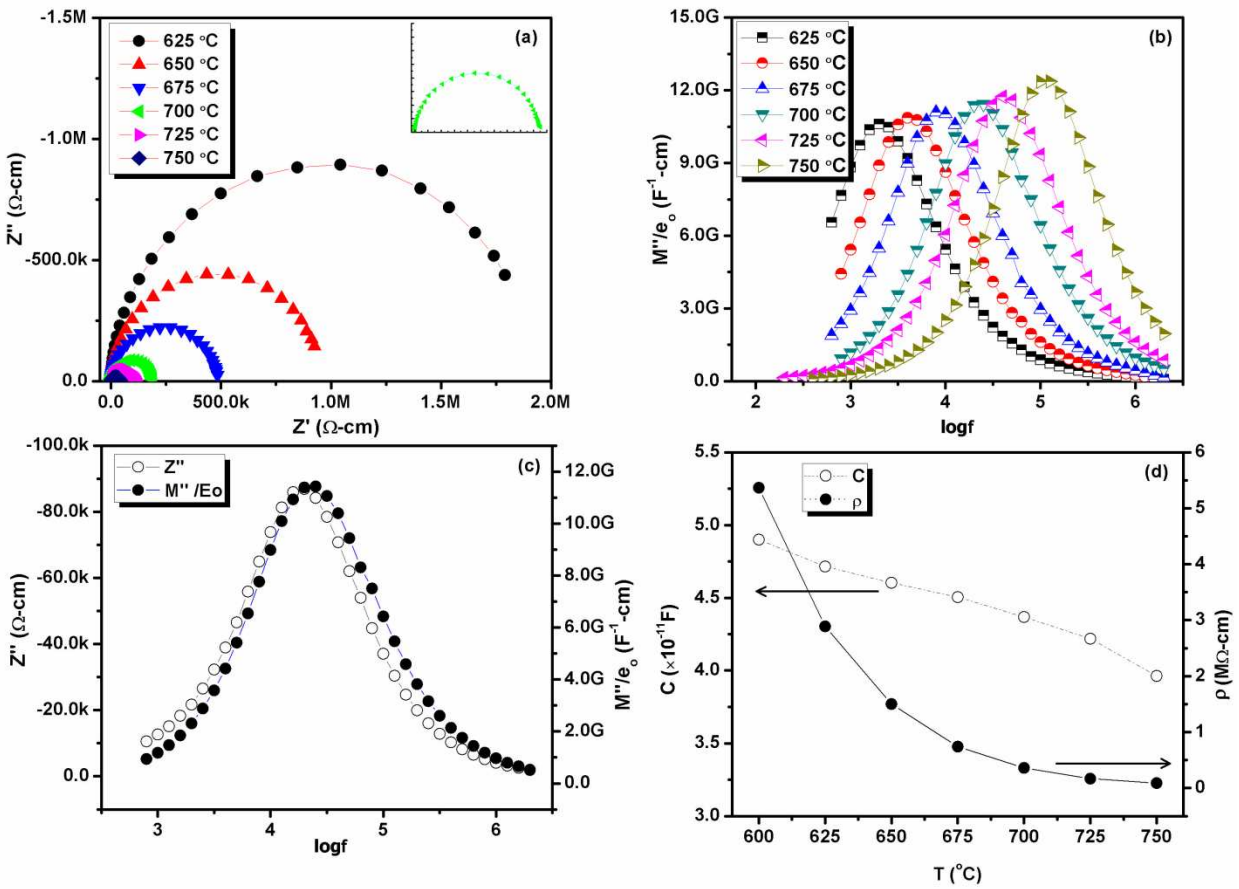

Fig. 6. a) Nyquist plot, b) spectroscopic plot log(f) versus M''/ε_o, c) plot of Z'' and M''/ε_o versus frequency and d) frequency dependent capacitance and resistivity of the x = 0.5 sample

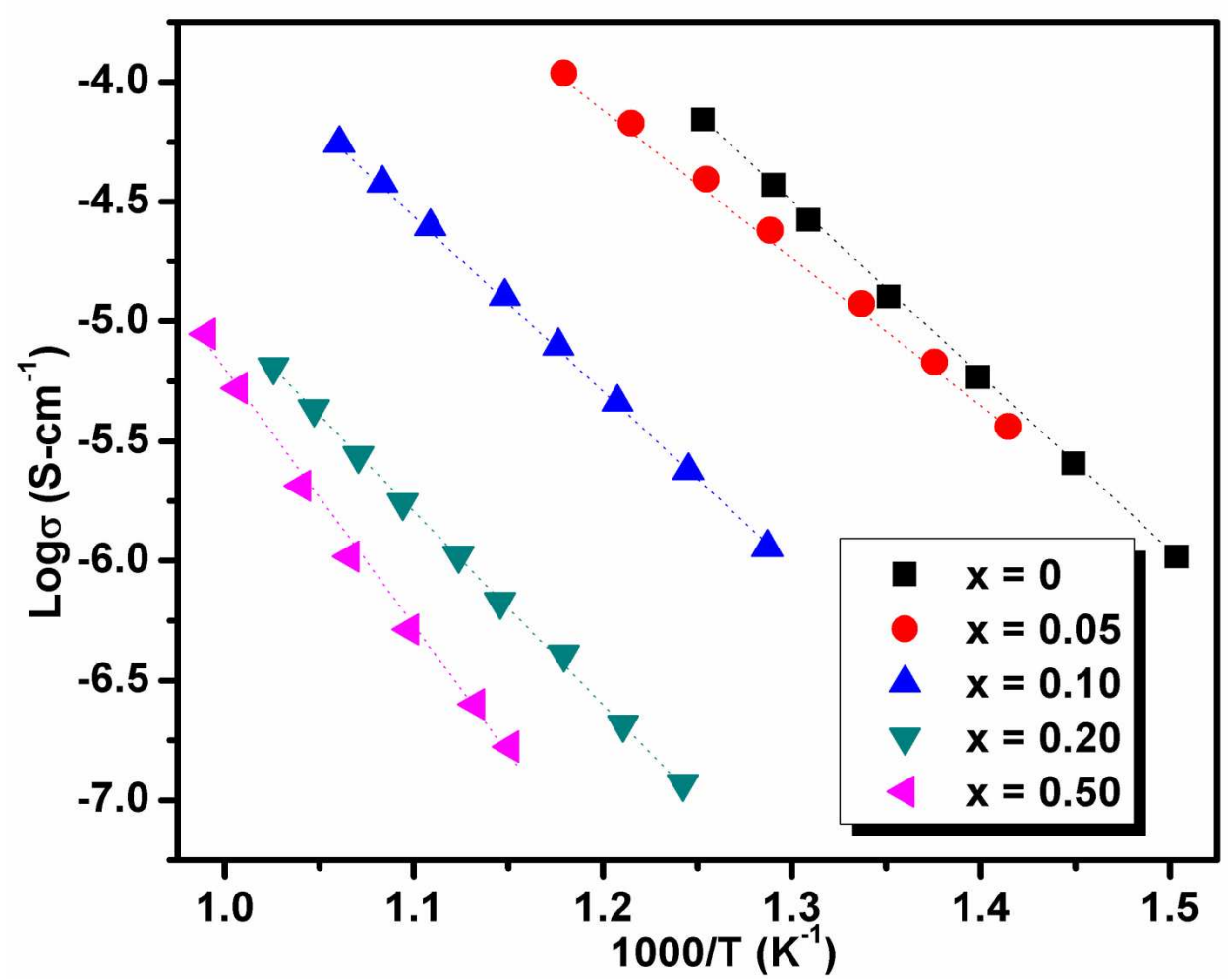

Fig. 7. Arrhenius plot of conductivity of (1-x)$BaTiO_3$–x$Bi(Mg_{2/3}Nb_{1/3})O_3$ (x = 0-0.6)